Energy transport in one-dimensional disordered granular solids

V. Achilleos,[1] G. Theocharis,[1] and Ch. Skokos[2]
[1]*LUNAM Université, LAUM, Université du Maine, UMR No. 6613, CNRS, Avenue O. Messiaen, 72085 Le Mans, France*
[2]*Department of Mathematics and Applied Mathematics, University of Cape Town, Rondebosch 7701, South Africa*
(Received 10 September 2015; published 12 February 2016)

We investigate the energy transport in one-dimensional disordered granular solids by extensive numerical simulations. In particular, we consider the case of a polydisperse granular chain composed of spherical beads of the same material and with radii taken from a random distribution. We start by examining the linear case, in which it is known that the energy transport strongly depends on the type of initial conditions. Thus, we consider two sets of initial conditions: an initial displacement and an initial momentum excitation of a single bead. After establishing the regime of sufficiently strong disorder, we focus our study on the role of nonlinearity for both sets of initial conditions. By increasing the initial excitation amplitudes we are able to identify three distinct dynamical regimes with different energy transport properties: a near linear, a weakly nonlinear, and a highly nonlinear regime. Although energy spreading is found to be increasing for higher nonlinearities, in the weakly nonlinear regime no clear asymptotic behavior of the spreading is found. In this regime, we additionally find that energy, initially trapped in a localized region, can be eventually detrapped and this has a direct influence on the fluctuations of the energy spreading. We also demonstrate that in the highly nonlinear regime, the differences in energy transport between the two sets of initial conditions vanish. Actually, in this regime the energy is almost ballistically transported through shocklike excitations.

DOI: 10.1103/PhysRevE.93.022903

I. INTRODUCTION

Wave scattering and energy transport in disordered media have for a long time been a matter of great research interest [1]. The experimental observation of Anderson localization in different systems such as optical systems [2], ultracold atomic gases [3], and elastic networks [4] has renewed the research in this direction. In addition, recent studies on wave scattering in random media have lead to a plethora of applications in imaging, random lasing, and solar energy (see, for example, [5] and references therein).

The key phenomenon employed in these studies is the spatial wave localization due to disorder, which is a linear effect relying on keeping phase coherence of participating waves [6]. However, wave localization can also emerge due to nonlinearity, as it was first shown in the studies of Fermi-Pasta-Ulam (FPU) [7], and may lead to energy localization and propagation through the formation of localized solutions (solitons, breathers, etc.) in different lattice models [8]. The interplay of these two localization mechanisms, nonlinearity and disorder, has been studied extensively in recent years [9–27]. In most of these studies, an initially localized wave packet was shown to lead to delocalization and a subdiffusive spreading of the energy, for sufficiently large nonlinearities. The most common models that have been studied are the Klein-Gordon model and the discrete nonlinear Schrödinger model; the latter in particular has attracted much attention due to its application to various optical structures and devices. Experimental studies on optical structures show that nonlinearity can either enhance localization (for focusing nonlinearity) or induce delocalization (for defocusing nonlinearity) [28,29].

Granular solids, namely, densely packed arrays of macroscopic particles that appear naturally disordered, are a promising test bed for studying the interplay of disorder and nonlinearity. The latter originates from the interparticle Hertzian contacts [30]. An especially appealing characteristic of these media is their tunable dynamical response ranging from near linear to highly nonlinear, by changing the ratio of static to dynamic interparticle displacements. Fabricated granular solids have allowed the exploration of a plethora of fundamental phenomena, including solitary waves with a highly localized waveform in the case of uncompressed crystal and discrete breathers [31–38]. They have been applied also in various engineering devices, including shock and energy absorbing layers [36,39,40], acoustic lenses [41], and acoustic diodes [42].

For sufficiently weak excitations and in the presence of precompression, the one-dimensional disordered granular solid, also called a granular chain, can be approximated by a disorder harmonic lattice, which has some interesting transport properties. In particular, it has been shown that different initial conditions, i.e., initial displacement or momentum excitations, of a single particle can lead to subdiffusive (displacement) or superdiffusive (momentum) energy transport [43], as well as to analytical described asymptotic energy profiles [26]. On the other hand, for sufficiently strong excitations or in the absence of precompression, the granular chain exhibits two different types of nonlinearity: (i) a power nonlinearity stemming from the Hertzian contacts and (ii) a nonsmooth nonlinearity, which is triggered whenever two beads of the chain lose contact (gap opening). The latter is present in a broad class of fragile mechanical systems that lose rigidity upon lowering the external pressure towards zero, such as weakly connected polymers [44] and network glasses [45]. It is also present in cracked solids [46].

Recently, studies of one-dimensional disordered granular chains have been reported [47–49]. In the absence of precompression, when the *nonsmooth nonlinearity* is present, it was shown that if a solitary wave is formed, it features an exponential decay that strongly depends on the degree of randomness [48,49]. Similar results were also reported in a two-dimensional granular solid [50] where the decay of the amplitude of the wave front was described using an

analogy between disorder and viscoelastic dissipation. On the other hand, in the presence of precompression, the power nonlinearity stemming from the Hertzian contacts leads to a FPU-like dynamics, which has been studied theoretically in the presence of disorder [24–26]. However, in the case of granular chains, this dynamics can be strongly modified by the presence of the opening of gaps. Thus, the interplay of these two nonlinear mechanisms is of particular interest and it can drastically change the transport properties.

Only recently, a study about one-dimensional and pre-compressed random dimer granular chains [51] has reported some features of the energy transport. In this work, the authors compare wave dynamics in chains with three different types of disorder: an uncorrelated (Anderson-like) disorder and two types of correlated disorder. For the Anderson-like uncorrelated disorder, they found a transition from subdiffusive to superdiffusive dynamics depending on the amount of precompression in the chain. In the present work we consider a different kind of uncorrelated disorder (i.e., polydispersity through disorder in the bead radius) and we study both displacement and momentum initial excitations, emphasizing their differences and similarities [52]. In particular, we consider polydisperse disordered granular chains composed of spherical beads of the same material and with radii taken from a random distribution. Our motivation is the fact that most of the granular materials occurring in nature and industrial application are composed of a broad range of particle sizes [53]. By considering a single central bead excitation, we study the transport of energy in these disordered granular chains.

In Sec. II we present the equations of motion in a normalized form, define the conserved energy of the system, and also describe the parameters used for the characterization of the energy transport. Results for the linear case are shown in Sec. III, where the influence of the strength of the disorder on the dynamics is studied. In Sec. IV we show the main results of this work for the case of an initial displacement excitation and explicitly identify three different regions of energy transport, a near linear regime, a weakly nonlinear regime, and a highly nonlinear regime. The energy transport for the case of an initial momentum excitation is discussed in Sec. V, presenting differences from and similarities to the initial displacement excitation. Results concerning the limiting profile of the energy for the two types of initial conditions are given in Sec. VI. We summarize our results in Sec. VII.

II. DISORDERED GRANULAR CHAIN

We consider a one-dimensional chain consisting of $N+2$ spherical beads, with masses m_n ($n = 0,1,2,\ldots,N+1$) and Hertzian contacts as shown in Fig. 1. We consider fixed boundary conditions for the first and last spherical beads, namely, $u_0 = u_{N+1} = 0$, where u_n is the displacement of each bead from its equilibrium position. Then the system is described by the following set of differential equations:

$$\begin{aligned} m_1\ddot{u}_1 &= A_1[\delta_1 - u_1]_+^{3/2} - A_2[\delta_2 + u_1 - u_2]_+^{3/2}, \\ m_n\ddot{u}_n &= A_n[\delta_n + u_{n-1} - u_n]_+^{3/2} - A_{n+1}[\delta_{n+1} + u_n - u_{n+1}]_+^{3/2}, \\ m_N\ddot{u}_N &= A_N[\delta_N + u_{N-1} - u_N]_+^{3/2} - A_{N+1}[\delta_{N+1} + u_N]_+^{3/2}, \end{aligned} \tag{1}$$

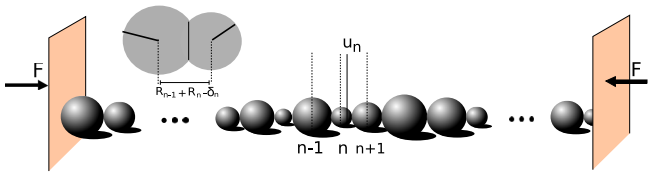

FIG. 1. Sketch of a granular chain with beads of random radius. Here u_n denotes the displacement of each bead from its equilibrium position, while δ_n is the overlap between two spherical beads due to the precompression force F.

where A_n is the contact coefficient between beads $n-1$ and n and δ_n is the relative static overlap due to a precompression force F acting on the two boundaries. The dots denote differentiation with respect to time. The coefficient A_n for spherical beads of the same material is given by $A_n = (2/3)\mathcal{E}\sqrt{(R_{n-1}R_n)/(R_{n-1}+R_n)}/(1-\nu^2)$ [30], where $\mathcal{E}$ and ν are the elastic modulus and Poisson's ratio respectively and R_n is the radius of the nth bead. The static overlap δ_n is given by $\delta_n = (F/A_n)^{2/3}$ [30]. The $[\,]_+$ sign in Eq. (1) denotes the following: When the expression inside the square brackets becomes negative (i.e., the beads are not in contact) this term becomes zero. In fact, this happens when the relative displacement between two beads becomes larger than their overlap $u_{n-1} - u_n > \delta_n$, that is, there is a *gap* between them, and their relative force vanishes.

Below we will work in dimensionless units, however for clarity we note that we use a reference radius of $R = 0.01$ m, a static force of $F = 1$ N, and stainless steel spherical beads (316 type), the elastic modulus of which is $\mathcal{E} = 193$ GPa while the Poisson ratio is $\nu = 0.3$. Relevant experiments with granular chains containing few defects can be found in [54]. In the following we will consider a disordered setup where the radii R_n of the different beads will be taken as a random variable, with values taken from a uniform distribution within the range $R_n \in [R,\alpha R]$, where the parameter $\alpha \geqslant 1$ describes the disorder strength. Consequently, the mean value $\tilde{R}$ of the bead radius is $\tilde{R} = (\alpha+1)R/2$. In order to make our equations dimensionless we implement the following transformations for time, distance, mass, and stiffness, respectively:

$$\begin{aligned} t \to \tilde{\omega}t, \quad \delta_n \to \delta_n/\tilde{\delta}\ (u_n \to u_n/\tilde{\delta}), \\ m_n \to m_n/\tilde{m}, \quad A_n \to A_n/6\tilde{A}, \end{aligned} \tag{2}$$

where all the quantities with a tilde are calculated at $\tilde{R}$. The frequency $\tilde{\omega}_c = (6\tilde{A}\tilde{\delta}^{1/2}/\tilde{m})^{1/2}$ is the maximum allowed propagative frequency of a monatomic chain with spherical beads of radius $\tilde{R}$. The normalization is such that in the case of no disorder ($\alpha = 1$) the *normalized* cutoff frequency is $\omega_c = 1$. The energy of the system is given by the following expression:

$$E = \sum_{n=1}^{N} E_n \equiv \sum_{n=1}^{N}\left(\frac{p_n^2}{2m_n} + V_n\right), \tag{3}$$

where E_n and $p_n = m_n\dot{u}_n$ are the energy and momentum of the nth bead, respectively. The potential V_n for each spherical

bead is defined as $V_n = [V(u_n) + V(u_{n+1})]/2$, where

$$V(u_n) = \frac{2}{5}A_n[\delta_n + u_{n-1} - u_n]_+^{5/2} - \frac{2}{5}A_n\delta_n^{5/2} - A_n\delta_n^{3/2}(u_{n-1} - u_n). \quad (4)$$

To study the energy transport in this one-dimensional system we focus on the time evolution of the second moment of the energy distribution [26] defined as

$$m_2 = \frac{\sum_n |n - n_0|^2 h_n(t)}{E}, \quad (5)$$

where $n_0 = N/2$ corresponds to the central bead of the chain and $N = 2 \times 10^4$ to the total number of spherical beads. In this last expression, $h_n = E_n/E$ denotes the portion of the total energy E acquired by the nth bead. Another useful quantity that characterizes the system is the participation number

$$P = 1 \Big/ \sum_n h_n^2, \quad (6)$$

which measures the number of excited beads that significantly contribute in the energy distribution. It takes the value $P = 1$ if all the energy is concentrated in one bead while it becomes $P = N$ in the case of energy equipartition. In our study we investigate the energy transport under two different sets of initial conditions: (i) $u_{N/2}(0) = u$, $u_{n\neq N/2}(0) = 0$, and $\dot{u}_n(0) = 0$ and (ii) $u_n(0) = 0, \dot{u}_{N/2}(0) = \dot{u}$, and $\dot{u}_{n\neq N/2}(0) = 0$, corresponding, respectively, to an initial *displacement* and an initial *momentum* excitation of the central bead. We present results obtained by averaging over 200 disorder realizations. Throughout the text the average value over disorder realizations of a quantity x is denoted by $\langle x \rangle$. Simulations are carried out using the SABA2C symplectic integrator, which allows us to keep the relative energy error at the order of 10^{-4} [13,55]. We also note that in our simulations energy never reaches the boundaries of the chain.

III. HARMONIC CHAIN

For sufficiently small displacements, i.e., $u_{n-1} - u_n \ll \delta_n$, the system of equations (1) can be approximated by the following linear system:

$$m_n\ddot{u}_n = K_n(u_{n-1} - u_n) - K_{n+1}(u_n - u_{n+1}), \quad (7)$$

where $K_n = (3/2)A_n\delta_n^{1/2}$ is the linear coupling constant. In the absence of disorder $\alpha = 1$, the energy spreading is ballistic and the second moment grows in time as $m_2(t) \propto t^2$, while $\langle P \rangle$ diverges for both displacement and momentum initial excitations. On the other hand, for the case of randomly chosen radii, Eq. (7) has the form of a disordered harmonic chain. This system has already been studied in several works [26,43,56] with either a mass disorder or a disorder in the coupling constants K_n. For the granular chain considered here, having beads of the same material but of different radius, both the masses m_n and the coupling constants K_n are random variables (both depend on the radius of the beads). Since masses depend on the radius as $m \propto R^3$, while the linear couplings as $K \propto R^{1/3}$, we expect that the disorder effect is stronger due to the masses.

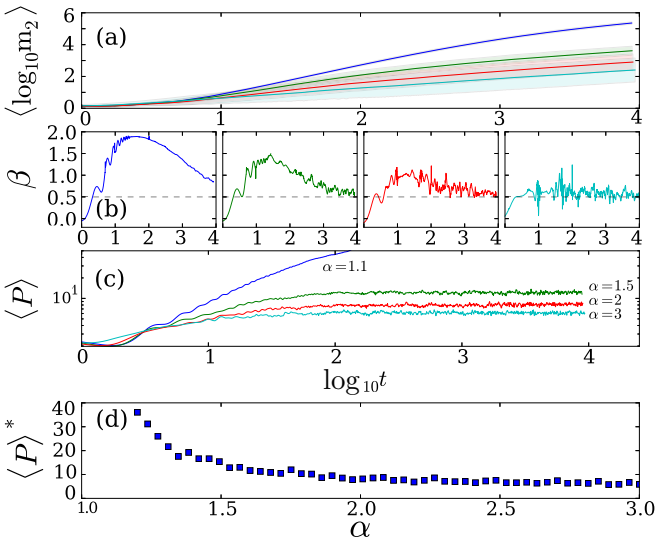

FIG. 2. Harmonic chain. (a) Time evolution of $\langle \log_{10} m_2(t) \rangle$ for different values of α. The shaded area corresponds to the standard mean deviation of the measured mean value. Curves from top to bottom correspond to $\alpha = 1.1, 1.5, 2, 3$, respectively. (b) Time derivative β of $\langle \log_{10} m_2(t) \rangle$ given by Eq. (8) as a function of $\log_{10} t$ for $\alpha = 1.1, 1.5, 2, 3$ from left to right. The horizontal dashed lines indicate the value $\beta = 0.5$. (c) Time evolution of the mean participation number $\langle P \rangle$ for the different values of the disorder parameter α. Curves from top to bottom correspond to $\alpha = 1.1, 1.5, 2, 3$, respectively. (d) Limiting value of the mean participation number $\langle P \rangle^*$ as a function of α.

In order to investigate the importance of the disorder parameter α on the system's behavior, we numerically integrate Eq. (7) for different values of α and the results are presented in Fig. 2. In particular, in Fig. 2(a) we show the time evolution of the average logarithm of the second moment $\langle \log_{10} m_2(t) \rangle$ with respect to the logarithm of time. Furthermore, in the panels of Fig. 2(b) we show the time evolution of β, the time derivative of $\langle \log_{10} m_2(t) \rangle$ given by

$$\beta = \frac{d\langle \log_{10} m_2 \rangle}{d \log_{10} t}. \quad (8)$$

The derivative is calculated numerically as follows: First we smooth the values of $\langle \log_{10}(m_2) \rangle$ by using a locally weighted regression algorithm [57] and then we apply an eighth-order central finite-difference scheme to compute the derivative. In [26,43] it was shown that for an initial displacement the energy transport is subdiffusive. In particular, the second moment grows in time as $m_2(t) \sim t^\beta$ with an asymptotic value for the exponent $\beta(t \to \infty) \sim 0.5$. From the first (leftmost) panel of Fig. 2(b) its readily seen that for $\alpha = 1.1$ the parameter $\beta(t)$ initially acquires a value close to $\beta = 2$, indicating a ballistic spreading of energy, but eventually it drops to smaller values, implying a slower spreading. However, one cannot induce a clear subdiffusive behavior for the time scales of our simulations. The second and third panels of Fig. 2(b) correspond to stronger disorder ($\alpha = 1.5$ and 2, respectively) where the tendency of β to asymptotically reach the value of $\beta = 0.5$ is evident, although some larger fluctuations are present. In the rightmost panel of Fig. 2(b), we plot the case

of $\alpha = 3$; we see that the value of β saturates to $\beta = 0.5$ very fast. However, we also notice that for this value of α, the fluctuations are even larger and this is also depicted by the very large standard deviation in the mean value of $\langle \log_{10} m_2(t) \rangle$, indicated by the shaded area around the lowest curve of Fig. 2(a). Therefore, a much larger number of realizations is needed for a better analysis of the $\alpha = 3$ case.

The respective mean participation number $\langle P \rangle$ for the different values of the disorder parameter α is shown in Fig. 2(c). For $\alpha = 1.1$, the mean participation number does not saturate, at least on the times of our simulations. On the other hand, for stronger disorder, e.g., $\alpha = 2$, it acquires a limiting value depending on the disorder parameter. The dependence of the numerical estimation of the limiting value of $\langle P(t \to \infty) \rangle = \langle P \rangle^*$ for different values of α is shown in Fig. 2(d). These estimations are obtained using the results of Fig. 2(c) as the mean value of $\langle P \rangle$ at the second half of the last decade of the simulation, i.e., for $5 \times 10^3 \leqslant t \leqslant 10^4$. Thus we may identify a weak disorder regime ($\alpha \lesssim 1.5$), where $\langle P \rangle^*$ has a value larger than 10 and approaches the total number of particles N in the case of no disorder ($\alpha = 1$), and a strong disorder regime ($\alpha > 1.5$), where it saturates to values of about ten beads or fewer. For this reason and due to the fact that for values $\alpha \geqslant 3$ the smoothing of large fluctuations of the computed quantities would imply many more disorder realizations, we restrict our analysis to the disorder regime with $\alpha = 2$.

We note that results similar to the ones of Fig. 2 were obtained for the case of initial momentum excitation. In particular, we recovered that the asymptotic value of β is 1.5, in the case of $\alpha = 2$. In the rest of this work we systematically investigate the effect of the nonlinearity on our system.

IV. DISPLACEMENT EXCITATION

In this section we present our findings for the transport of energy induced by an initial displacement of the central spherical bead in the chain. Typical results of the dynamics observed for different amplitudes of the initial displacements are shown in Fig. 3. The top and middle panels illustrate clearly that a localized state is formed near the initially excited bead, while there are two propagating fronts traveling towards the edges of the chain. These results show that for an increasing amplitude of the initial excitation, these fronts are found to be propagating faster. In the bottom panel, which corresponds to $u = 10$, the behavior is significantly altered, since now the energy looks to be more equally distributed through the lattice. This fact is better illustrated by looking at the insets (on the right-hand side of each panel), where we show the corresponding energy profile at a late time instant $t = 2 \times 10^3$ for each case. For the cases of the top and middle panels, it can be readily seen that the energy around the initially excited bead is almost five orders of magnitude larger than the energy of more distant beads. On the other hand, in the bottom panel the differences of energy between the central region and the rest of the chain are significantly smaller.

In what follows we discuss in more detail the outcomes of extensive numerical simulations for several values of the nonlinearity strength. The main results are summarized in Fig. 4. In particular, in Fig. 4(a) we plot the time evolution of

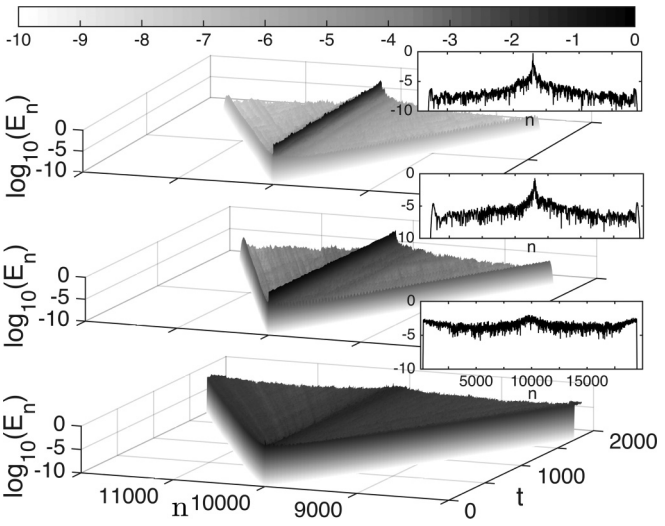

FIG. 3. Time evolution of the logarithm of the energy E_n of a portion of the chain near the initially excited bead at $n = N/2 = 10^4$. Different panels (from top to bottom) correspond to different values of the initial displacement u and in particular to $u = 0.01$, 1, and 10, respectively. The coloring of each lattice site, according to the color scale shown on top of the panels, denotes the $\log_{10}(E_n)$ value of the corresponding bead. The insets on the right of each panel show the corresponding energy profile at a late time instant $t = 2 \times 10^3$.

$\langle \log_{10} m_2 \rangle$, in Fig. 4(b) we plot the time evolution of its time derivative, and in Fig. 4(c) we show the mean participation number $\langle P \rangle$ as a function of time.

A. Near linear regime

Let us first note that for values of the initial excitation $u < 0.1$ [see, e.g., the blue (lowest) line in Fig. 4(b), which corresponds to $u = 0.01$], we observe that $\beta \approx 0.5$ at about $t \approx 10^4$. Additionally, the mean participation number for this case [Fig. 4(c)] is found to practically saturate to the same value as in the harmonic chain. Thus, we conclude that for values of $u < 0.1$ the nonlinear model is characterized by a

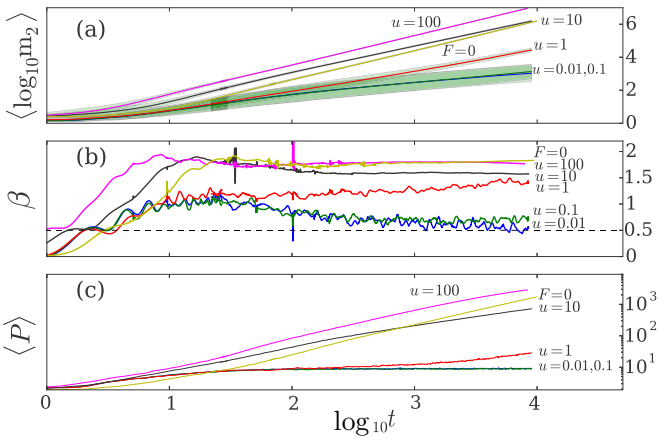

FIG. 4. Time evolution of (a) the averaged logarithm of the second moment $\langle \log_{10} m_2 \rangle$ for different initial displacements u, (b) the time derivative $\beta(t)$ of the respective curves of (a), and (c) the mean value of the participation number $\langle P \rangle$.

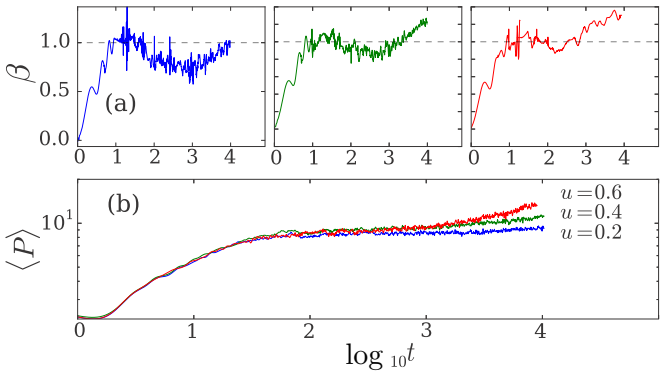

FIG. 5. (a) Time evolution of the parameter β for different values of the initial displacement excitation $u = 0.2,0.4,0,6$ (from left to right) in the regime where energy transport crosses from subdiffusive to superdiffusive behavior. The horizontal dashed lines indicate the value $\beta = 1$. (b) Time evolution of the mean participation number for displacement excitations corresponding to the top panels.

near linear regime, having qualitatively and quantitatively the same energy transport properties as its linear counterpart, at least for the time scales of our simulations.

B. Weakly nonlinear regime

From the results of Fig. 4 it can be readily seen that already for an initial condition of $u = 0.1$, the value of β deviates from its behavior in the linear case, becoming larger than 0.5. However, a very abrupt change in the behavior of β is observed at the value $u = 1$ and the system undergoes a transition from subdiffusion to superdiffusion. Notice also that, although for $u = 0.1$ the mean participation number in Fig. 4(c) saturates to a value of $\langle P\rangle \approx 10$, for the value $u = 1$ it is found to continuously increase. These two results indicate the existence of a regime of intermediate dynamics for values between $u = 0.1$ and 1.

In order to further understand the dynamics in this regime, we compute the parameter β, as well as the mean participation number $\langle P\rangle$, for some intermediate values of initial displacements, i.e., $u = 0.2,0.4,0.6$. The results obtained, which are plotted in Fig. 5, clearly show that a transition from subdiffusion to superdiffusion is carried out in this regime. In Fig. 5(a) the parameter β exhibits many fluctuations and shows no evident tendency to saturate into a constant value until the end of our numerical simulations. In all cases shown in Fig. 5(a), β initially approaches the diffusive value $\beta = 1$ but later starts to decrease. Furthermore, at a time interval between $t \approx 10^2$ and 10^3 it saturates to an almost constant value somewhat below $\beta = 1$, but eventually the dynamics changes and β starts to increase again, becoming larger than 1. This behavior creates a characteristic local minimum of $\beta(t)$ for all studied cases shown in Fig. 5. This result is in accord with the recent study of [26], where it was found that in the FPU problem, until the end of the times studied, there was no clear limiting value for the exponent of m_2.

It is also relevant to discuss the behavior of the mean participation number $\langle P\rangle$ in this weakly nonlinear regime. As it is shown in Fig. 5(b), after an initial increase of $\langle P\rangle$ its value remains practically constant with a value of around

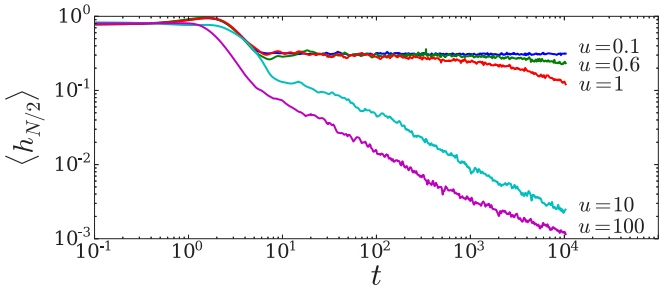

FIG. 6. Normalized mean energy $\langle h_{N/2}\rangle$ of the central bead at $n = N/2$ as a function of time for different initial displacements; from top to bottom, $u = 0.1,0.6,1,10,100$.

$\langle P\rangle \approx 10$, between $t \approx 10^2$ and 10^3, but after this time interval $\langle P\rangle$ increases, exhibiting a diverging trend. This transition is attributed to nonlinearity, since it is never observed in the near linear regime or in the exact linear case. To further understand the origin of this behavior, we plot in Fig. 6 the normalized mean energy of the central bead $\langle h_{N/2}\rangle$ as a function of time. For $u = 0.1$ after a small transient time of $t \approx 10$, the central bead retains a large amount of the total energy of the system, keeping it up to the end of our simulations at $t = 10^4$. This behavior is understood by the fact that most of the energy is concentrated around the initially excited bead, due to the presence of the disorder-induced localized modes. These modes remain localized throughout the simulation. However, for larger values of the initial excitation, i.e., $0.1 < u \lesssim 1$, we observe that, although for a large time interval ($10 \lesssim t \lesssim 10^3$) most of the energy is trapped around the central bead, after sufficient time the energy of this bead starts to decrease. This signals the detrapping of energy from this bead and its release to the rest of the chain.

C. Highly nonlinear regime

For even larger values of the initial condition $u > 1$, i.e., for larger nonlinearities, we observe in Fig. 4 that the exponent β saturates to an almost constant value at about $t \approx 10^2$ describing a superdiffusive regime. These values are larger with respect to the values of β seen in the weakly nonlinear regime. It is worth noting that in this regime the fluctuations in the values of β are much smaller than in the previous regime. From Fig. 6 we also conclude that the normalized mean energy of the central bead $\langle h_{N/2}\rangle$ for $u = 10,100$ continuously decreases as a function of time, in contrast with the weakly nonlinear regime. To further investigate the dynamics in this regime we evaluate the probability of gap openings between beads as obtained by counting the number of gaps in each site for all 200 disorder realizations and plot in Fig. 7 the average value obtained. In great contrast to the weakly nonlinear regime where no gaps appear, here we find that not only are there always many gaps around the initially excited bead, but also these gaps propagate in the system. This observation strongly suggests that for such large initial excitations, a different dynamical regime is present, where the dynamics is governed not by the FPU-like nonlinearity but by the nonsmooth nonlinearity of the opening of gaps. We call this regime highly nonlinear.

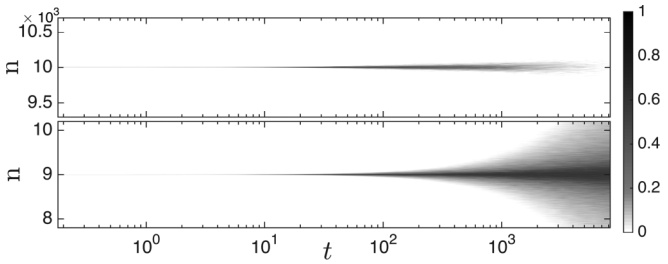

FIG. 7. Probability of a gap opening as a function of time for two different initial displacements in the highly nonlinear regime: $u = 10$ (top panel) and $u = 100$ (bottom panel). We focus on the dynamics around the central bead $N/2$. The black in the color map corresponds to probability 1 while the white to 0.

A particular limit of this highly nonlinear regime corresponds to the case of $F = 0$, which results in $\delta_n = 0$ in Eq. (1). This is also called a sonic vacuum [31] due to the fact that the system does not support the propagation of linear waves. This regime has been studied extensively for the case of no disorder, namely, when $\alpha = 1$. It is known that a solitary solution exists in this limit with a highly localized waveform [31]. For the case of a binary system with a disordered distribution between beads of two different masses, similar solitary waves of decreasing amplitude were found in the weak disorder limit, while in the strong disorder case a delocalized wave was observed [49]. Similar results were obtained for the case of two-dimensional granular solids, with an initial excitation only in one direction: Weak disorder induces an exponentially decreasing solitary wave that eventually gives its place to a delocalized shocklike profile, while strong disorder only exhibits a shocklike structure [50,58]. The latter works also showed that at the position n_f of the front of the shocklike structure, the velocity scales as $\dot{u}_f \propto n_f^{-1/2}$.

Let us now explore the transition from the highly nonlinear regime to the singular case of $F = 0$. First note that, as shown in Fig. 4(b), for $F = 0$ the exponent β reaches the value $\beta \approx 1.8$, which is the maximum value, while the mean participation number is qualitatively similar for all the cases in the highly nonlinear regime. Furthermore, in Fig. 8 we plot the velocity profiles at five time instants for the case of $F = 0$ with $u = 1$ and for the case of $F \neq 0$ with $u = 10$ and 100. For $F = 0$, in agreement with [50,58], we observe the formation of a propagating front with a characteristic triangular profile, which

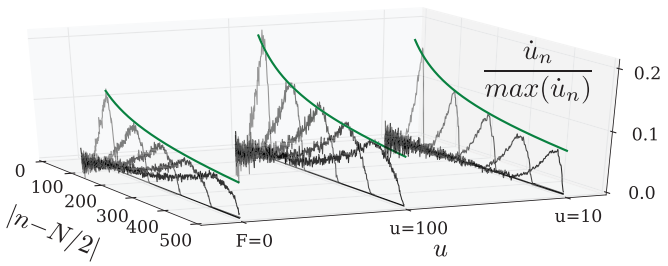

FIG. 8. Velocity profiles $\dot{u}_n$ for five time instants, normalized to its maximum value for different initial conditions. Shown on the left is the case of $F = 0$ with $u = 1$; the middle and right show the case of $F \neq 0$ with $u = 100$ and 10, respectively.

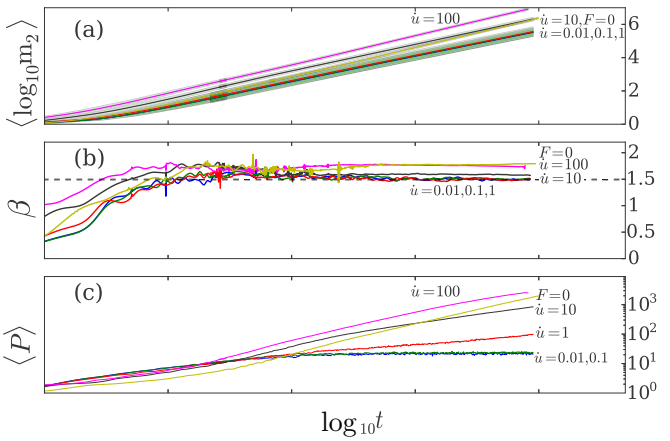

FIG. 9. Same as in Fig. 4 but for different initial momentum excitations $\dot{u}_{N/2}(0) = \dot{u}$.

however becomes less sharp in time (see the leftmost case in Fig. 8). In fact, by plotting a fitting curve of the form $n_f^{-1/2}$, shown as an envelope on top of the velocity profiles [solid (green) line], it can be clearly seen that the propagating front follows this $-1/2$ power law trend.

More importantly, we find that even in the case of a finite precompression force $F \neq 0$, a similar structure can be formed and is propagating with the same power law decay of its amplitude (see the middle case in Fig. 8). However, for the case of $u = 10$, although the peak of the propagating form seems to follow a similar trend, the observed structure is different: It does not exhibit a long tail that terminates at the central bead ($n = N/2$), but it exhibits a finite width of the order of 100 beads (see the rightmost case in Fig. 8).

V. MOMENTUM EXCITATION

As we mentioned in the Introduction, the energy transport in disordered linear chains strongly depends on the initial condition [26,43]. Thus, in order to complete the dynamical study of our model we also investigate the case of an initial momentum excitation of the central spherical bead by increasing the initial velocity $\dot{u}_{N/2}(0) = \dot{u}$. The results are summarized in Figs. 9 and 10.

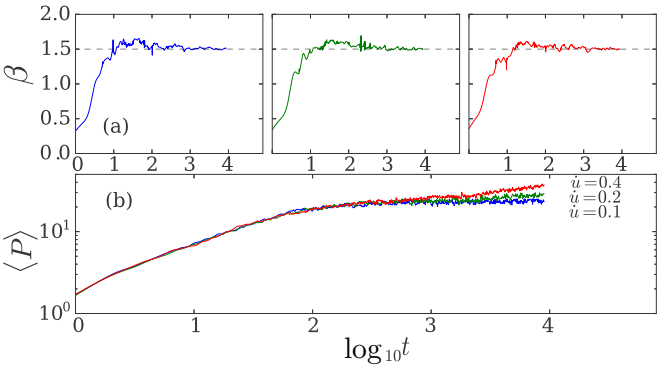

FIG. 10. Same as in Fig. 5 but for different initial momentum excitations $\dot{u}_{N/2}(0) = \dot{u}$. The top panels correspond to $\dot{u} = 0.1, 0.2, 0.4$ from left to right.

In the linear case the energy spreading for an initial momentum excitation is known to be superdiffusive with $\beta = 1.5$ [43]. By numerical simulations of the normalized nonlinear equations of motion (1), we found that the energy spreading remains superdiffusive with $\beta = 1.5$ for all initial velocities $\dot{u} < 10$ [see Figs. 9(b) and 10(a)]. This is in contrast to the case of the initial displacement excitation, where the relevant values of β exhibit large variations. For $\dot{u} \gtrsim 10$ the exponent β grows and eventually reaches the maximum value of $\beta \approx 1.8$, which is also the corresponding value of β of the limiting case of $F = 0$. We again identify this regime as the highly nonlinear regime.

On the other hand, the mean participation number $\langle P \rangle$ exhibits behavior similar to the case of initial displacement excitations. For $\dot{u} \lesssim 0.1$ it saturates to a constant value of about 20 beads, while for $\dot{u} > 0.1$ it continuously increases. Looking closer to $\langle P \rangle$, shown in Fig. 10(b), we note that the mean participation number reaches the limiting constant value of about 20 beads for $\dot{u} = 0.1$, i.e., the near linear regime. However, for $\dot{u} = 0.2,0.4$, although it seems to saturate to a constant value for a long time, finally it starts to deviate and increase continuously. This again suggests that there is an intermediate regime for $0.1 < \dot{u} \lesssim 1$ in which energy detrapping is observed. This is the weakly nonlinear regime.

To conclude, compared to the case of displacement initial excitations, there is a difference in the energy transport properties in the intermediate regime that we call weakly nonlinear. Although the mean participation number $\langle P \rangle$ shows the same behavior, in contrast to the displacement excitations, for momentum initial excitations both the near linear and weakly nonlinear regimes are characterized by an asymptotic value of the parameter $\beta = 1.5$, namely, the same as for the linear case.

Another interesting point to be mentioned is that, although in the linear case the energy transfer is subdiffusive or superdiffusive for an initial displacement or an initial momentum excitation, respectively, in the highly nonlinear regime and more profoundly in the limiting case of $F = 0$ both excitations result in the same behavior of energy transport. In fact, in this limit, not only the limiting value of β (as it was also found in Ref. [52] for a disordered dimer), but also the dynamics of the derivative β of $\langle m_2 \rangle$ are very similar.

VI. ASYMPTOTIC PROFILES

According to Ref. [26], the asymptotic dependence of the energy moments (not only m_2) can be characterized by the asymptotic energy profile of the lattice, at least in the linear case. In particular, it was shown in that work that the energy profile far away from the central excitation has the form $\langle h_n \rangle \sim |n - N/2|^{-\eta}$. The exponent η was found to be $\eta = 5/2$ and $3/2$ for displacement and momentum initial excitations, respectively. In Fig. 11 we show for both displacement (top panels) and momentum initial excitations (bottom panels) three different instants of the energy profile at sufficiently large times, covering all the dynamical regimes from near linear (left column) to highly nonlinear (right column). In the left panels (near linear regime) it can be readily seen that, in accord with the predictions for the linear problem, the three profiles are almost identical, indicating the fact that the energy distribution has reached a limiting profile that does not change for later times. For comparison, we plot curves (dashed lines) with a slope of $5/2$ (top) and $3/2$ (bottom). Note also that the energy distribution near the central bead (i.e., for $n \approx N/2$ in the figure) is the same for the three different profiles. This indicates that the energy of these sites also does not change in time and the mode around the center remains localized.

The top (bottom) second column panel of Fig. 11 depicts the energy profile for an initial displacement (momentum) excitation with $u = 1$ ($\dot{u} = 1$). In this case it can be readily seen that for the initial displacement excitation (top) the three profiles do not overlap and also the slopes are not exactly $5/2$. This is another indication for the appearance of the weakly nonlinear regime that exhibits nontrivial dynamics. Note that for the momentum excitation (bottom) the profiles do overlap. This is in accord with the discussion in Sec. V about the

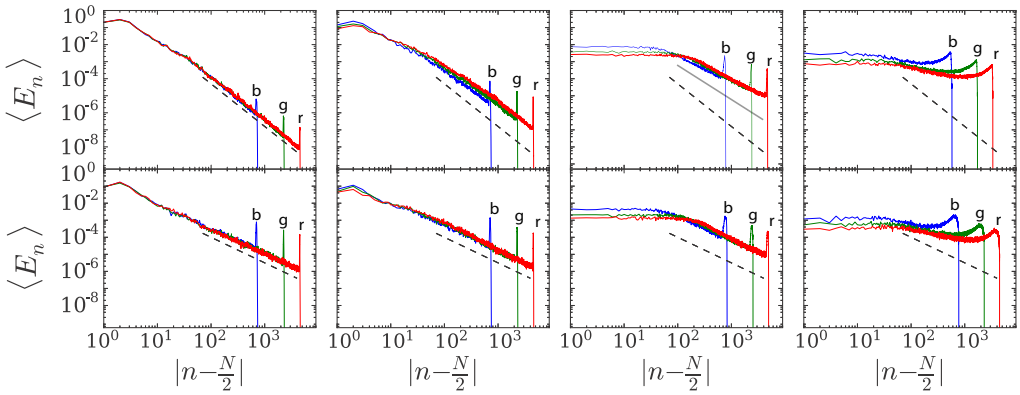

FIG. 11. Profiles of the energy distribution for initial displacement (top panels) and momentum (bottom panels) excitation. The values of the initial displacement excitations are $u = 0.01,1,10$ for the first three top panels (from left to right) and $u = 1$ when $F = 0$ for the fourth top panel. The values of the initial momentum excitations are $\dot{u} = 0.01,1,10$ for the first three top panels (from left to right) and $\dot{u} = 1$ when $F = 0$ for the fourth top panel. These values cover all the dynamical regimes: from the near linear (left column) to the highly nonlinear (right column) regime. The different profiles are taken at times $t \approx 1500$ (curve b, blue), $t \approx 5000$ (curve g, green), and $t \approx 10\,000$ (curve r, red). The dashed lines denote slopes of $5/2$ (top) and $3/2$ (bottom). For the top third panel, the additional solid line denotes the slope of $3/2$.

limiting value of β, which is the same for both the near linear and the weakly nonlinear regime. Additionally, for both cases of initial conditions, we observe a small but non-negligible deviation of the energy around the center, which confirms the fact that the localized mode around the center starts to lose its energy.

For larger values of the initial condition as shown in the top (bottom) third column panel of Fig. 11, the profile of the energy is substantially different. It is characterized by two different regimes: a weakly localized part with almost 10^2 beads with a similar amount of energy, forming an almost straight horizontal line, and a decaying tail. However, the weakly localized portion of the energy is spreading and loses its energy, as for larger times the almost straight horizontal part of the profile becomes longer, having smaller energy values. We also note that once again the slope of the energy profiles for initial displacements (top panel) is not $5/2$ as time increases but interestingly enough it reaches a value that is closer to $3/2$ (see the gray solid line). We recall that for this initial displacement excitation with $u = 10$, β asymptotically reaches the value of 1.5 (see Fig. 4), which is also the limiting value of β of an initial momentum excitation of the linear problem.

Finally, for the particular case of $F = 0$, as shown in the top (bottom) fourth column panel of Fig. 11, the asymptotic energy profile is similar to a ballistic propagation where the energy differences between excited beads decrease drastically, but in this case the propagating front does not exhibit a sharp profile. In fact, this front has a very large tail that is due to the shocklike structure that was mentioned in Sec. IV C.

VII. CONCLUSION

In this work we numerically investigated the energy transport in a one-dimensional granular solid composed of spherical beads of randomly distributed radii that interact via Hertzian forces. We studied the dynamics by using two different localized initial conditions, i.e., initial displacement and initial velocity excitations of the central bead of the chain, and by increasing the amplitude of these excitations. We were able to identify three different dynamical spreading regimes with distinct characteristics: the near linear, the weakly nonlinear, and the highly nonlinear.

In the near linear regime, part of the initial energy remains localized around the central excited bead while two counterpropagating fronts, coherent phonons, travel through the chain. We found that the energy transport is identical to that of a linear chain, with either mass or coupling disorder, at least up to the time scales reached in our simulations. The spreading of the energy is characterized by an asymptotic time dependence of the mean second moment of the energy m_2 of the form $\langle m_2 \rangle \sim t^{\beta}$, where $\beta = 0.5$ and 1.5 for an initial displacement and an initial momentum excitation, respectively. Additionally, the mean participation number $\langle P \rangle$ in this regime converges to a constant value, which depends on the strength of the disorder.

For larger values of the initial conditions, in the weakly nonlinear regime, we found that for initial displacement excitations the energy spreading does not exhibit a clear asymptotic time dependence. However, it does cross to a superdiffusive behavior, since for large enough time scales, the slope of m_2 becomes larger than 1. In fact, this behavior, which was also observed in the study of [26] for a FPU lattice, is found to be closely connected to the nonlinear dynamics of the localized state formed around the central spherical bead. We found that after a sufficient time interval [between 10^2 and 10^3 normalized time units; see Eq. (2)], the central localized region consisting of about ten beads starts to delocalize and the energy stored in these spherical beads starts to radiate into the system. In this weakly nonlinear regime, the dynamics is governed by the power Hertzian nonlinearity. On the other hand, for initial momentum excitations, the slope of m_2 remains around 1.5, as in the near linear regime, but $\langle P \rangle$ exhibits the same behavior as for displacement excitations.

For even larger amplitudes of the initial excitation, the energy transfer becomes substantially different. The energy profile of the chain reveals an almost ballistic behavior with an almost equal distribution of the energy around the excited portion of the chain. In this regime, which we characterized as highly nonlinear, the system exhibits a large number of gaps between beads, which is a nonsmooth nonlinear process. We found that these gaps propagate in the chain and that the transport of energy is mediated by a shocklike structure, which bares similarities to the self-similar solution found in [58].

An important result of our work is the following: Although it is known that the energy transport for the disordered linear chain strongly depends on the type of initial conditions (i.e., displacement or momentum excitations), we found that in the highly nonlinear regime it is independent of the initial condition. This is probably a rather general feature of disordered granular chains as it was very recently observed in different disordered dimer granular chain [52]. In particular, in the linear case the asymptotic time dependence of $\langle m_2 \rangle$ shows a slope of $\beta = 0.5$ (displacement) and $\beta = 1.5$ (momentum), while for the extreme nonlinear limit of $F = 0$ both initial conditions lead to a slope of $\beta \approx 1.8$. Additionally, the energy profiles in this regime show that there is no distinct localized state.

ACKNOWLEDGMENTS

G.T. acknowledges financial support from FP7-People-2013-CIG grant, Project No. 618322 ComGranSol. Ch.S. was partially supported by the National Research Foundation of South Africa (Incentive Funding for Rated Researchers). We thank the anonymous referees whose remarks helped us improve the clarity of the paper. Ch.S. thanks LAUM for its hospitality during his visits when part of this work was carried out.

[1] P. Sheng, *Introduction to Wave Scattering, Localization and Mesoscopic Phenomena* (Springer, Berlin, 2006); B. van Tiggelen and S. Skipetrov, *Wave Scattering in Complex Media: From Theory to Applications* (Springer, Dordrecht, 2003).

[2] D. S. Wiersma, P. Bartolini, A. Lagendijk, and R. Righini, Nature (London) **390**, 671 (1997); A. A. Chabanov, M. Stoytchev, and A. Z. Genack, *ibid.* **404**, 850 (2000); M. Störzer, P. Gross, C. M. Aegerter, and G. Maret, Phys. Rev. Lett. **96**, 063904 (2006).

[3] J. Billy, V. Josse, Z. Zuo, A. Bernard, B. Hambrecht, P. Lugan, D. Clement, L. Sanchez-Palencia, P. Bouyer, and A. Aspect, Nature (London) **453**, 891 (2008); G. Roati, C. D'Errico, L. Fallani, M. Fattori, C. Fort, M. Zaccanti, G. Modugno, M. Modugno, and M. Inguscio, *ibid.* **453**, 895 (2008); S. S. Kondov, W. R. McGehee, J. J. Zirbel, and B. DeMarco, Science **334**, 66 (2011).

[4] H. Hu, A. Strybulevych, J. H. Page, S. E. Skipetrov, and B. A. van Tiggelen, Nat. Phys. **4**, 945 (2008).

[5] Diederik S. Wiersma, Nat. Photon. **7**, 188 (2013); J.-H. Park, C. Park, H. S. Yu, J. Park, S. Han, J. Shin, S. H. Ko, K. T. Nam, Y.-H. Cho, and Y. K. Park, *ibid.* **7**, 454 (2013); B. Redding, S. F. Liew, R. Sarma, and H. Cao, *ibid.* **7**, 746 (2013).

[6] P. W. Anderson, Phys. Rev. **109**, 1492 (1958).

[7] *The Fermi-Pasta-Ulam Problem: A Status Report*, edited by G. Gallavotti, Lecture Notes in Physics Vol. 728 (Springer, Heidelberg, 2010).

[8] P. Kevrikidis, J. Appl. Math. **76**, 3 (2011).

[9] M. I. Molina, Phys. Rev. B **58**, 12547 (1998).

[10] A. S. Pikovsky and D. L. Shepelyansky, Phys. Rev. Lett. **100**, 094101 (2008).

[11] G. Kopidakis, S. Komineas, S. Flach, and S. Aubry, Phys. Rev. Lett. **100**, 084103 (2008).

[12] S. Flach, D. O. Krimer, and Ch. Skokos, Phys. Rev. Lett. **102**, 024101 (2009).

[13] C. Skokos, D. O. Krimer, S. Komineas, and S. Flach, Phys. Rev. E **79**, 056211 (2009).

[14] H. Veksler, Y. Krivolapov, and S. Fishman, Phys. Rev. E **80**, 037201 (2009).

[15] M. Mulansky, K. Ahnert, A. Pikovsky, and D. L. Shepelyansky, Phys. Rev. E **80**, 056212 (2009).

[16] C. Skokos and S. Flach, Phys. Rev. E **82**, 016208 (2010).

[17] S. Flach, Chem. Phys. **375**, 548 (2010).

[18] T. V. Laptyeva, J. D. Bodyfelt, D. O. Krimer, C. Skokos, and S. Flach, Europhys. Lett. **91**, 30001 (2010).

[19] J. D. Bodyfelt, T. V. Laptyeva, G. Gligoric, D. O. Krimer, C. Skokos, and S. Flach, Int. J. Bifurcat. Chaos **21**, 2107 (2011).

[20] J. D. Bodyfelt, T. V. Laptyeva, C. Skokos, D. O. Krimer, and S. Flach, Phys. Rev. E **84**, 016205 (2011).

[21] D. Basko, Ann. Phys. (NY) **326**, 1577 (2011).

[22] B. Vermersch and J. C. Garreau, Phys. Rev. E **85**, 046213 (2012).

[23] T. Kottos and B. Shapiro, Phys. Rev. E **83**, 062103 (2011).

[24] R. Bourbonnais and R. Maynard, Phys. Rev. Lett. **64**, 1397 (1990).

[25] G. S. Zavt, M. Wagner, and A. Lütze, Phys. Rev. E **47**, 4108 (1993).

[26] S. Lepri, R. Schilling, and S. Aubry, Phys. Rev. E **82**, 056602 (2010).

[27] T. V. Laptyeva, M. V. Ivanchenko, and S. Flach, J. Phys. A **47**, 493001 (2014).

[28] T. Pertsch, U. Peschel, J. Kobelke, K. Schuster, H. Bartelt, S. Nolte, A. Tünnermann, and F. Lederer, Phys. Rev. Lett. **93**, 053901 (2004).

[29] Y. Lahini, A. Avidan, F. Pozzi, M. Sorel, R. Morandotti, D. N. Christodoulides, and Y. Silberberg, Phys. Rev. Lett. **100**, 013906 (2008).

[30] K. L. Johnson, *Contact Mechanics* (Cambridge University Press, Cambridge, 1985); V. F. Nesterenko, *Dynamics of Heterogeneous Materials* (Springer, Berlin, 2001).

[31] V. F. Nesterenko, J. Appl. Mech. Tech. Phys. **24**, 733 (1984).

[32] C. Coste, E. Falcon, and S. Fauve, Phys. Rev. E **56**, 6104 (1997).

[33] E. B. Herbold, J. Kim, V. F. Nesterenko, S. Y. Wang, and C. Daraio, Acta Mech. **205**, 85 (2009).

[34] A. C. Hladky-Hennion and M. de Billy, J. Acoust. Soc. Am. **122**, 2594 (2007).

[35] N. Boechler, G. Theocharis, S. Job, P. G. Kevrekidis, M. A. Porter, and C. Daraio, Phys. Rev. Lett. **104**, 244302 (2010).

[36] J. Hon, Phys. Rev. Lett. **94**, 108001 (2005).

[37] S. Job, F. Santibanez, F. Tapia, and F. Melo, Phys. Rev. E **80**, 025602 (2009).

[38] G. Theocharis, N. Boechler, and C. Daraio, *Acoustic Metamaterials and Phononic Crystals* (Springer, New York, 2013), pp. 217–251.

[39] C. Daraio, V. F. Nesterenko, E. B. Herbold, and S. Jin, Phys. Rev. Lett. **96**, 058002 (2006).

[40] R. Doney and S. Sen, Phys. Rev. Lett. **97**, 155502 (2006).

[41] A. Spadoni and C. Daraio, Proc. Natl. Acad. Sci. USA **107**, 7230 (2010).

[42] N. Boechler, G. Theocharis, and C. Daraio, Nat. Mater. **10**, 665 (2011).

[43] P. K. Datta and K. Kundu, Phys. Rev. B **51**, 6287 (1995).

[44] C. P. Broedersz and F. C. MacKintosh, Rev. Mod. Phys. **86**, 995 (2014).

[45] J. C. Phillips, J. Non-Cryst. Solids **43**, 37 (1981).

[46] S. Mezil, N. Chigarev, V. Tournat, and V. Gusev, Opt. Lett. **36**, 3449 (2011).

[47] B. P. Lawney and S. Luding, Acta Mech. **225**, 2385 (2014).

[48] M. Manjunath, A. P. Awasthi, and P. H. Geubelle, Phys. Rev. E **85**, 031308 (2012).

[49] L. Ponson, N. Boechler, Y. M. Lai, M. A. Porter, P. G. Kevrekidis, and C. Daraio, Phys. Rev. E **82**, 021301 (2010).

[50] N. Upadhyaya, L. R. Gómez, and V. Vitelli, Phys. Rev. X **4**, 011045 (2014).

[51] A. J. Martínez, P. G. Kevrekidis, and M. A. Porter, Phys. Rev. E **93**, 022902 (2016).

[52] In a second version of Ref. [51], A. J. Martínez, P. G. Kevrekidis, and M. A. Porter, arXiv:1411.5746v2, which appeared after the submission of this paper, the authors also considered the case of initial momentum excitation, obtaining some results that are in agreement with the relevant results of this work.

[53] J. K. Mitchell and K. Soga, *Fundamentals of Soil Behavior*, 3rd ed. (Wiley, New York, 2005); T. Aste and D. Weaire, *The Pursuit of Perfect Packing* (Institute of Physics, Bristol, 2000).

[54] Y. Man, N. Boechler, G. Theocharis, P. G. Kevrekidis, and C. Daraio, Phys. Rev. E **85**, 037601 (2012).

[55] J. Laskar and P. Robutel, Celest. Mech. Dyn. Astron. **80**, 39 (2001).

[56] K. Ishii, Prog. Theor. Phys. Suppl. **53**, 77 (1973).

[57] W. S. Cleveland and S. Devlin, J. Am. Stat. Assoc. **83**, 596 (1988).

[58] B. E. McDonald and D. Calvo, Phys. Rev. E **85**, 066602 (2012).